


Martini Force Field for Protonated Polyethyleneimine

Titus Adrian Beu ,* Andrada-Elena Ailenei, and Răzvan-Ioan Costinaș

Polyethyleneimine (PEI), one of the most widely used nonviral gene carriers, was investigated in the presented work at coarse-grained (CG) level. The main focus was on elaborating a realistic CG force field (FF) aimed to reproduce dynamic structural features of protonated PEI chains and, furthermore, to enable massive simulations of DNA–PEI complex formation and condensation. We parametrized CG Martini FF models for PEI in polarizable and non-polarizable water by applying Boltzmann inversion techniques to all-atom (AA) probability distributions for distances, angles, and

dihedrals of entire monomers. The fine-tuning of the FFs was achieved by fitting simulated CG gyration radii and end-to-end distances to their AA counterparts. The developed Martini FF models are shown to be well suited for realistic large-scale simulations of size/protonation-dependent behavior of solvated PEI chains, either individually or as part of DNA–PEI systems. © 2019 Wiley Periodicals, Inc.

DOI: 10.1002/jcc.26110

Introduction

Its remarkable properties and straightforward fabrication have currently turned polyethyleneimine (PEI), $-\text{[CH}_2\text{—NH—CH}_2\text{]}_n-$, into one of the most commonly used nonviral gene delivery vectors. The particular interest in polyplexes formed by PEI and DNA stems from their low toxicity and the appreciable transfection efficiency that can be achieved by optimizing the protonation pattern of PEI. It is commonly accepted that the formation and condensation of these polyplexes, apt to enter cells via endocytosis, are conditioned to a large extent by the electrostatic interactions occurring between the positive amino groups of protonated PEI monomers, $-\text{CH}_2-\text{NH}_2^+-\text{CH}_2-$, and the negative phosphate groups of DNA.

There is presently a vivid experimental and theoretical interest in optimizing the formation and condensation of DNA–PEI polyplexes.^[1–3] Experimental studies have conclusively proven both the high efficiency of PEI as genetic vector and the low cytotoxicity of the formed DNA–PEI complexes. For example, DNA condensation enabled by PEI chains as part of a mixture of cationic agents and trivalent ions was reported by Jorge et al.^[4] to show increased efficiency in the presence of Fe ions. In the context of cancer immunotherapy, Cai et al.^[5] have very recently built nanocomposites formed of PEI and inorganic materials as gene delivery systems and proved their transfection efficiency via fluorescence microscopy.

Analyzing the formation of small DNA–PEI complexes at all-atom (AA) level by molecular dynamics (MD) requires moderate computational resources. Nevertheless, when it comes to in-depth investigations of the mechanisms governing DNA–PEI polyplex condensation, the number of atoms rapidly exceeds tens of millions, and systematic AA MD simulations become cumbersome even for high-performance computer systems. In such cases, resorting to coarse-grained (CG) models (by mapping entire atom groups into single “beads”), if realistically parametrized, appears to be the method of choice, typically reducing the number of simulated particles by an order of magnitude and

enabling significantly increased simulation times as a result of the reduced computational costs (due to less simulated particles, consideration of only short-range interactions, and stability for substantially larger time steps).

Ziebarth and Wang^[6] already studied a decade ago the condensation of DNA with PEI–polyethylene glycol (PEG) diblock copolymers via CG MD simulations. Using a simple bead-spring model for the polymers, they presented conclusions on the degree of condensation and structure of the formed complexes in dependence on the cationic block length and linear versus star-shaped structure of the copolymers.

More recently, Wei and Luijten^[7] developed an AA CHARMM (Chemistry at Harvard Macromolecular Mechanics) force field (FF) for PEG-grafted linear PEI by applying a “divide-and-conquer” strategy to small building blocks and optimizing the dihedral parameters relative to ab initio potential energy scans. The resulted AA FF was used in simulations of complexation of small interfering RNA (siRNA) with PEG-grafted PEI. AA distributions of bonds, angles, and dihedrals from simulations of isolated PEG-grafted PEI in water served as input for the parametrization of a CG model, by repeatedly adjusting the CG parameters so as to achieve a good match between the CG and AA distributions. The standard Martini types assigned by Wei and Luijten to the beads for fixing the nonbonded interactions and are found to match one of the optimal combinations found in the present work.

Carrillo et al.^[8] performed MD CG simulations of branched PEIs as part of silica mesoporous supports. Similarly to Ziebarth

[a] T. A. Beu, A.-E. Ailenei, R. Costinaș
Faculty of Physics, Department of Biomolecular Physics, University Babeș-Bolyai, Mihail Kogălniceanu Street 1, Cluj-Napoca 400084, Romania
E-mail: titus.beu@phys.ubbcluj.ro

Contract Grant sponsor: Unitatea Executiva pentru Finantarea Invatamantului Superior, a Cercetarii, Dezvoltarii si Inovarii; Contract Grant number: Project PN-III-P4-ID-PCE-2016-0474; Contract Grant sponsor: Romanian National Authority for Scientific Research and Innovation, CNCS

© 2019 Wiley Periodicals, Inc.

and Wang, they used the bead-spring model for the aminopolymers.

Very recently, Mahajan and Tang^[9] published a CG Martini FF for PEI in linear and branched configurations, which relies on (asymmetric) beads corresponding to C–C–N groups. The parametrization of this CG FF was carried out by Boltzmann inversion, using reference distributions resulted from simulations performed using the AA FF reported by Sun et al.^[10] This AA FF essentially adopts residues by analogy from the CHARMM27 FF,^[11] lacking a specific parametrization for bonds and angles, while optimizing only the torsional parameters by fits to ab initio data. For comparison reasons, we specifically consider in our investigations the choice of Mahajan and Tang for the standard Martini types attributed to the PEI beads.

An increasingly accepted *general strategy* for developing CG models, which we actually adopted in our line of studies regarding PEI over the last couple of years, involves operating at three distinct levels (length scales):

1. Ab initio: Provides accurate quantum mechanical reference data from calculations on sets of PEI models featuring the typical vicinity for each relevant atomic species. Generic system sizes are of the order of 25 Å and around 50 atoms.
2. Atomistic (AA): Involves developing AA FFs (e.g., CHARMM^[11–13]) based on the QM reference data produced within step 1. Fine-tuning and validation of the FFs are achieved by matching MD simulation results to experimental data. Typical system sizes for solvated PEI chains are of the order of 100 Å and 100,000 atoms.
3. Coarse-grained (CG): Involves parametrizing CG FFs (e.g., Martini^[14–17]) using AA probability distributions for bead interdistances, angles, and dihedrals. Fine-tuning and validation of the CG FF are done by matching CG structural features with AA simulations and experimental data. System sizes in DNA–PEI condensation simulations typically exceed 250 Å and 500,000 beads (the equivalent of about 2,000,000 atoms).

Covering the first two steps, while aiming to develop a more realistic AA FF for PEI than its predecessors, we have recently published two variants of a CHARMM FF,^[1,2] one based on *asymmetric* residues (with –C–C–N– backbones), and a thoroughly revised version based on *symmetric* residues (with –C–N–C– backbones), the latter being in many respects more appropriate with a view to developing a CG FF. A notable difference with respect to previous AA models for PEI was that we consistently adjusted not only the torsional parameters, but the *entire* set of bonded parameters, along with the partial atomic charges. The quality of the parametrization was underpinned by an extensive body of accurate reference ab initio data extracted from PEI model pentamers.

The present study takes a step forward, completing the third task of the general strategy for developing CG FFs for PEI. Specifically, we focused on developing Martini FF models, defining beads located at the mass centers of *symmetric* PEI monomers, –CH₂–NH–CH₂– and/or –CH₂–NH₂⁺–CH₂–. We generated reference distributions for interbead distances, angles, and dihedrals, as well as reference values for gyration radii, end-to-end distances, and diffusion coefficients from large ensembles of AA trajectories

run for three PEI sizes and four protonation fractions using our latest CHARMM model.^[2] The bonded parameters were determined from the AA distributions by Boltzmann inversion,^[18] comparatively via single-function and multifunction fits. For defining the nonbonded parameters, comprehensive CG MD simulations were performed for a wide range of standard Martini-type combinations assigned to the PEI beads, both with polarizable and nonpolarizable water. The root mean square deviations (RMSD) of the gyration radii and end-to-end distances between the entire CG and AA ensembles were used to choose the most appropriate standard Martini types. The optimal combinations of bonded and nonbonded (standard Martini) parameters were finally decided considering the best match between the CG and AA distributions for bead interdistances, angles, and dihedrals.

To further demonstrate the usefulness of the developed CG FF for PEI, we used it in conjunction with the Martini FF for DNA^[17] in modeling the formation of DNA–PEI complexes. We present complex formation results for a short DNA molecule (double dodecamer), leaving the bulk of the results for the condensation of significantly longer DNA strands for a follow-up paper, as well as the study of branched PEI polymers.

Methodology

Martini FF model

Martini^[14–17] is a versatile and increasingly popular additive CG model, successfully used in the last decade in MD simulations of large biomolecular systems. The Martini FF model operates with *beads* as units, often defined as entire functional groups, employing as a general rule a four-to-one mapping, which means that four heavy atoms (plus the associated hydrogens) are replaced by a single CG bead. The Martini FF model comprises bonded and nonbonded interactions:

$$U_{\text{bonded}} = \frac{1}{2} \sum_{\text{bonds}} K_b (b - b_0)^2 + \frac{1}{2} \sum_{\text{angles}} K_\theta (\theta - \theta_0)^2 + \sum_{\text{dihedrals}} K_\psi [1 + \cos(n\psi - \psi_0)], \quad (1)$$

$$U_{\text{nonbonded}} = \sum_{\text{beads } i, j} \left\{ \frac{q_i q_j}{4\pi\epsilon_0\epsilon_r r_{ij}} + 4\epsilon_{ij} \left[\left(\frac{\sigma_{ij}}{r_{ij}} \right)^{12} - \left(\frac{\sigma_{ij}}{r_{ij}} \right)^6 \right] \right\}. \quad (2)$$

The bonded terms model distances, angles, and dihedral angles between beads, whereby K_b , K_θ , and K_ψ are the corresponding force constants, while b_0 and θ_0 are, respectively, equilibrium distances and angles. To model multiwell potentials, the dihedral terms feature multiplicities n and reference phases ψ_0 . It should be noted that the original definition of the Martini angle-dependent terms is actually cos-harmonic, involving differences of cosines of angles, being used, for example, by Mahajan and Tang. However, for reasons of improving the agreement between AA and CG angular distributions, we adopted harmonic contributions in terms of angles as such.

The nonbonded terms account for electrostatic and van der Waals interactions, whereby q_i are bead charges, ϵ_{ij} are

Lennard-Jones (LJ) potential-well depths, and σ_{ij} are the corresponding zero-potential interbead distances.

The Martini model classifies the strength of the LJ non-bonded interactions by defining four basic bead types (Q—charged, P—polar, N—nonpolar, and C—apolar). The Q and N types have four subtypes (d—donor, a—acceptor, da—both, and 0—none) reflecting the bead's hydrogen-bonding capabilities, while the P and C types are subcategorized according to the degree of polarity (1–5). Additional “small” variants of the basic bead types, carrying a leading “S,” are introduced with reduced LJ parameters to allow for closer packing (e.g., in ring structures).^[15] Yet smaller “tiny” bead variants, carrying a leading “T,” are defined to quantify the van der Waals interactions of the nucleobases in DNA.^[17] The actual strength for each combination of standard bead types is specified by interaction tables and spans 10 levels, with well-defined LJ parameters.

The standard nonpolarizable Martini water is composed of neutral P4 beads, which represent groups of four water molecules. In order to break any spurious ordering and thus prevent artificial freezing, the P4 beads are replaced in a 1–10 ratio by (“big”) antifreeze particles BP4.

The polarizable Martini water model of Yesylevskyy et al.,^[19] useful for realistically modeling systems with pronounced charge separation, maps, just like the nonpolarizable model, four water molecules and comprises three beads: a neutral central bead and two beads of opposite fractional charge kept at fixed distance from the central one. The three beads share equally the mass of the four modeled water molecules and interact through a harmonic angular potential, creating a dipole moment responding to the local electric field. Recently, Michalowsky et al. published a reparametrized MARTINI model for polarizable water, with generally increased LJ interaction levels and optimized partial charges.^[20]

As per common practice, the Na^+ and Cl^- neutralizing ions are modeled as Qd and Qa (charged donor and acceptor) beads, respectively.

As explained in the “Results” section, we extracted the bonded parameters for the Martini model of PEI via Boltzmann inversion techniques^[18] from probability distributions of bead interdistances, angles, and dihedral angles, collected from large ensembles of AA trajectories for PEI chains of different lengths and (uniform) protonation fractions. As for defining realistic LJ interactions for the PEI beads, we scanned for the minimum of the RMSD between the CG and AA radii of gyration and end-to-end distances over a large set of standard Martini-type combinations, using both polarizable and nonpolarizable water.

MD simulations

All the AA MD simulations for solvated PEI chains referred to in this work are those published in our recent paper.^[2] They are based on our new CHARMM FF for PEI and were carried out using the NAMD (Nanoscale Molecular Dynamics) code.^[21] Essentially, we studied the structural and dynamical behavior of PEI chains composed of $12n + 3$ monomers, that is, the 27-mer, 39-mer, and 51-mer, respectively, denoted as PEI27, PEI39, and PEI51. The PEI chain sizes were chosen so as to allow for uniform

protonation in fractions 1/4 (one in four), 1/3 (one in three), and 1/2 (alternative protonation). The 12 PEI polymers combining the three chain sizes with the four protonation fractions (including no protonation) represent the reference simulation set (RSS) employed throughout in the present investigations to relate the AA and CG results. For each PEI polymer of the RSS, the performed NPT simulations (constant number of particles N , pressure P , and temperature T) spanned a total of 400 ns of data collection.

The bulk of the CG MD simulations reported here were carried out using Gromacs version 2018.1.^[22–24] For each polymer of the RSS, we generated NPT trajectories of 500 ns (preceded by 50 ps of equilibration) employing leap-frog propagation with a time step of 10 fs, and applied periodic boundary conditions in all directions using a 12 Å cutoff for the short-range interactions.

For treating electrostatics, we employed the reaction field method with a relative dielectric constant $\epsilon_r = 2.5$ in conjunction with polarizable water, an increased value $\epsilon_r = 15$, with standard water, and infinite screening beyond the cutoff distance. We also tested particle mesh Ewald electrostatics with a 1 Å grid spacing, however, without notable improvements to justify the increased computational effort.

The temperature was kept fixed at 310 K using stochastic velocity rescaling with a (weak) coupling constant of 1 ps, while the pressure was maintained at 1 bar via a Parrinello–Rahman barostat with a coupling constant of 12 ps.

The CG simulation box size for each polymer of the RSS was the same as in the corresponding AA simulations, being chosen so as to spaciouly accommodate the polymer coiled as a helix with the radius and axial extent of the order of the respective gyration radius. Specifically, the simulation boxes sizes were equal to 60, 75, and 90 Å for PEI27, PEI39, and PEI51, respectively, and the numbers of solvating water beads were about 1660, 3280, and 5700.

For selected FF models, we also performed comparative CG MD simulations with NAMD, which yielded for all polymers of the RSS similar results to those obtained with Gromacs, as expected.

Results and Discussion

Parametrization of the Martini model for PEI

For modeling our Martini FFs for PEI, we applied residue-based CG and defined three bead types (see Fig. 1), which exactly map the residues defined as part of our recent AA CHARMM FF model,^[2] being identified with the respective mass-centers and bearing the same names:

- PEI—generic nonprotonated PEI monomer $-\text{CH}_2-\text{NH}-\text{CH}_2-$.
- PEP—protonated PEI monomer $-\text{CH}_2-\text{NH}_2^+-\text{CH}_2-$.
- PEC— CH_3 group starting/ending PEI chains.

Indeed, from the perspective of the generic “four-to-one” mapping introduced by the Martini model, these beads appear to be rather small (the first two map just three heavy atoms, while the last, only one). It is, therefore, to be expected that, to

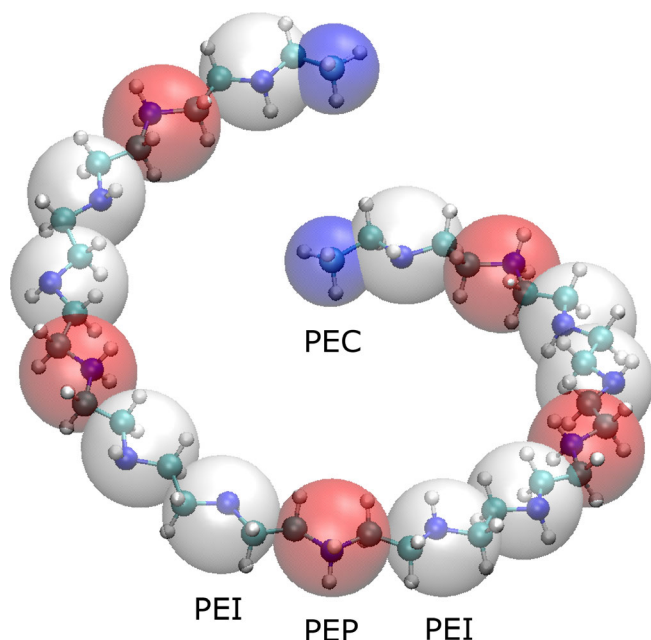


Figure 1. CG beads defined in our Martini FF model: PEI—unprotonated monomer $-\text{CH}_2-\text{NH}-\text{CH}_2-$ (white), PEP—protonated monomer $-\text{CH}_2-\text{NH}_2^+-\text{CH}_2-$ (red), and PEC—terminal methyl group (blue). [Color figure can be viewed at wileyonlinelibrary.com]

properly set the scale of their nonbonded interactions, these beads need to be identified with “small” standard Martini types.

We note that our *symmetric* bead mapping scheme with $-\text{C}-\text{N}-\text{C}-$ backbones is consistent with the one used by Wei and Luijten.^[7] By contrast, Mahajan and Tang^[9] based their mapping on the non-symmetric atomistic residues of Sun et al.^[10] with $-\text{C}-\text{C}-\text{N}-$ backbone.

Bonded parameters via Boltzmann inversion of atomistic distributions

It is obvious that in deconvoluting CG FF parameters from atomistic data, the bonded and nonbonded parameters cannot be uncoupled completely, and certain iterative refinement procedures may need to be applied. Anyhow, AA reference distributions for bead interdistances and angles are generally dominated by intramolecular bonding forces, depending less on van der Waals interactions. This creates the possibility for the CG bonded parameters, or at least very good initial approximations of theirs, to be by directly obtained by Boltzmann inversion^[18] of the AA profiles.

Another technical difficulty is that the AA distributions show by no means a single peak, as might be desirable for the straightforward application of the Boltzmann inversion, but generally have a multippeak structure reflecting the multiple “most-probable” conformers that occur in sampling the phase-space. Illustrative examples are the PEI–PEP distance (Fig. 2) and the PEI–PEP–PEI angle (Fig. 3), where the AA distributions (with triangles) clearly result from *three* independent Gaussian peaks (depicted with dotted lines), while none of these can be regarded as spurious. Since, by default, the established MD simulators (including Gromacs and NAMD) accept a unique force

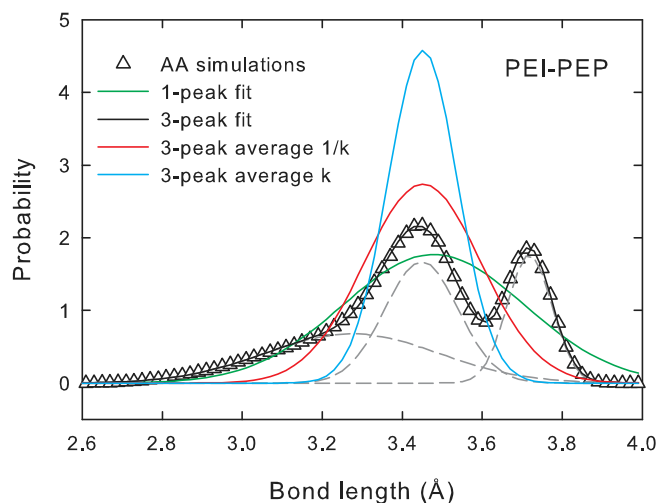


Figure 2. Atomistic probability distribution for the PEI–PEP bead distance (with triangles), 1-Gaussian fit (green line), 3-Gaussian fit (black line), 3-Gaussian average (red line) of inverse force constants [eq. (7)], and 3-Gaussian average (cyan line) of force constants. [Color figure can be viewed at wileyonlinelibrary.com]

constant/equilibrium value combination for each type of valence bond or angle bending coordinate, one needs to devise a more elaborate treatment than the simple single-Gaussian model.

One-Gaussian (1G) fit functions for the probability distributions of interbead distances b and angles θ ,

$$P = Ae^{-U/k_B T}, \quad (3)$$

with harmonic potential energy dependencies,

$$U_b = \frac{1}{2}K_b(b-b_0)^2, \quad U_\theta = \frac{1}{2}K_\theta(\theta-\theta_0)^2, \quad (4)$$

where k_B is Boltzmann’s constant and T is the equilibrium temperature, have a manifest tendency to produce too broad

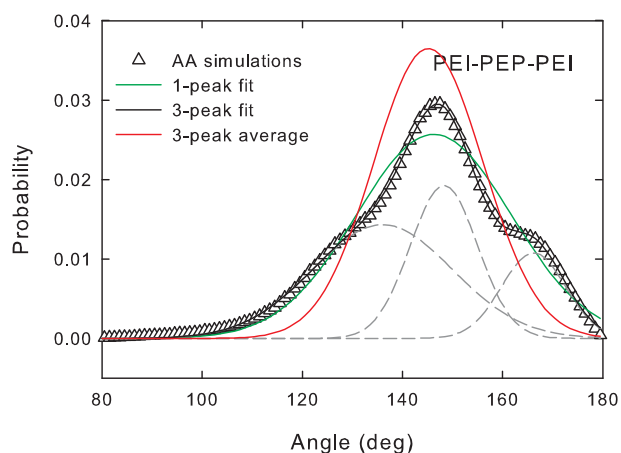


Figure 3. Atomistic probability distribution for the PEI–PEP–PEI angle (with triangles), 1-Gaussian fit (green line), 3-Gaussian fit (black line), and 3-Gaussian average (red line) of inverse force constants [eq. (8)]. [Color figure can be viewed at wileyonlinelibrary.com]

model profiles (with green continuous lines in Figs. 2 and 3) and much lower force constants than those corresponding to the individual peaks. From this perspective, three-Gaussian (3G) fit functions,

$$P = \sum_{i=1}^3 A_i e^{-U_i/k_B T} \quad (5)$$

with separate harmonic potential energy contributions,

$$U_{i,b} = \frac{1}{2} K_{b,i} (b - b_{0,i})^2, \quad U_{i,\theta} = \frac{1}{2} K_{\theta,i} (\theta - \theta_{0,i})^2 \quad (6)$$

appear to be more appropriate.

Specifically for the PEI–PEP distance (with two very well-separated peaks), the three force constants resulted from a 3G-fit are (from left to right) 5494, 30,104, and 81,734 kJ mol⁻¹ nm⁻², whereas the 1G-fit yields a smaller force constant (4999 kJ mol⁻¹ nm⁻²) than any of the previous ones. A particularly problematic situation is that of the PEC–PEI bond (see Supporting Information Fig. S1), where the two pronounced peaks in the AA distribution hardly show overlap so as to be identifiable with a single Gaussian function.

In adopting a multipeak approach, still the problem remains of how to combine the force constants and equilibrium distances/angles of the individual peaks into single values, as required by the analytical functional forms implemented in many commonly used MD codes. In order to maintain the analytic consistency of our Martini model, ultimately justified by the very good agreement between our simulated AA and CG structural data (such as gyration radii), but also ensuring wide compatibility with MD codes in use, we chose not to resort to tabulated potential energy functions, which, indeed, benefit from more flexibility, but lack enough portability across simulation communities. After testing several schemes, but minding that the squared peak half-widths relate inversely with the force constants, we settled on defining equivalent inverse force constants as weighted averages of the inverse individual force

constants (similar to springs connected in series), with the equilibrium distances and angles defined as simple weighted averages,

$$\frac{1}{K_b} = \sum_{i=1}^3 \frac{w_i}{K_{b,i}}, \quad b = \sum_{i=1}^3 w_i b_{0,i}, \quad (7)$$

$$\frac{1}{K_\theta} = \sum_{i=1}^3 \frac{w_i}{K_{\theta,i}}, \quad \theta = \sum_{i=1}^3 w_i \theta_{0,i}, \quad (8)$$

and weights proportional to the peak areas S_i ,

$$w_i = \frac{S_i}{\sum_i S_i}, \quad (9)$$

to better reflect the relative probabilities of the conformers. This 3G scheme generally results in larger force constants (narrower model peaks) than the 1G-fits. For the PEI–PEP distance, in particular, the 3G-fit leads to a force constant more than 2.4 times larger (12,117 kJ mol⁻¹ nm⁻²) and to more pronounced (red) model profiles in Figures 2 and 3. While the 3G-fits generally seem to closer reflect the overall AA probability distributions for bead inter-distances, the 1G-fits appear to work better for angles. It is, however, worth mentioning the case of the PEI–PEI–PEI angular distribution (Fig. S2), in which the 1G and 3G models result in very close profiles, with the corresponding force constants differing by less than 6%, and the equilibrium angles by roughly 1%.

A possibly more intuitive approach to produce single-valued force constants and positions would be to consider the straightforward weighted average of the individual force constants resulting from the 3G-fit (similar to springs in parallel), instead of their inverses. In the case of the PEI–PEP distance, this yields a significantly larger equivalent force constant (33,880 kJ mol⁻¹ nm⁻²) and the corresponding normalized profile (with cyan line in Fig. 2) appears too peaked, not realistically reflecting the overall AA distribution. For this reason we did not pursue this variant and considered further on, alongside the 1G-fit, only the 3G-inverse averaging scheme based on eqs.(7)–(9), in the following simply referred to as 3G-averaging.

The CG bonding parameters resulted by 1G-fit and 3G-averaging from the AA probability distributions compiled for the entire RSS are listed in Table 1, and one may notice (with the sole exception of the PEI–PEI–PEI angle, for which the two approaches yield comparable results) the significantly lower force constants produced by the 1G-fit, both for distances and angles.

Given the qualitatively different shape of the distributions for the dihedral angles ψ defined by four adjacent beads, shown for illustration in Figure 4 for the PEI–PEI–PEI–PEP dihedral, as well as the fact that the established MD codes accept multiple functions for torsional coordinates, we used in this case a four-function fit:

$$P_\psi = A e^{-U_\psi/k_B T}, \quad (10)$$

where

$$U_\psi = \sum_{i=1}^4 K_{\psi,i} [1 + \cos(n_i \psi - \psi_{0,i})], \quad (11)$$

Table 1. CG bonded parameters for bead distances (bonds) and angles resulted from AA distributions by Boltzmann inversion using: (a) 1-Gaussian (1G) fits and (b) 3-Gaussian (3G) fits and parameter averaging according to eqs. (7)–(9).

Bond	1G-fit		3G-average	
	b_0	K_b	b_0	K_b
PEI–PEI	0.3328	5910	0.3274	18,246
PEI–PEP	0.3479	4999	0.3451	12,117
PEI–PEC	0.2412	4446	0.2428	88,315
Angle	θ_0	K_θ	θ_0	K_θ
PEC–PEI–PEI	139.29	48.998	139.95	70.003
PEC–PEI–PEP	135.96	29.638	135.05	50.392
PEI–PEI–PEI	130.61	37.263	132.14	35.152
PEI–PEI–PEP	140.32	27.683	139.37	47.466
PEI–PEP–PEI	146.26	35.441	145.19	70.749
PEP–PEI–PEP	134.89	26.712	135.28	46.080

Equilibrium distances b_0 are in nm, the corresponding force constants K_b , in kJ (mol nm²)⁻¹, equilibrium angles θ_0 are in degrees, and the corresponding force constants K_θ , in kJ (mol deg²)⁻¹. In the 3G model, due to its very large force constant, the PEI–PEC distance can actually be constrained.

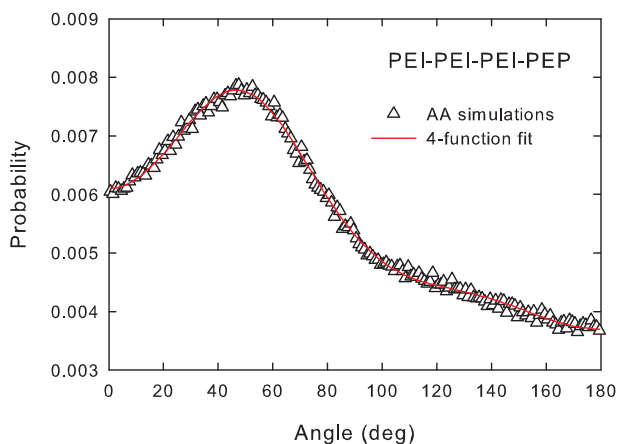


Figure 4. Atomistic probability distribution for the PEI-PEI-PEI-PEP dihedral angle (with triangles) and four-function fit (red line) [eqs. (10)–(11)]. [Color figure can be viewed at wileyonlinelibrary.com]

with multiplicities $n_i = 1, 2, 3, 4$ and shifts $\psi_{0,i} = 0^\circ$ or 180° . The CG torsional parameters obtained by applying this model to the AA distributions of dihedral angles for the entire RSS are listed in Table S1 and the much lower order of magnitude of the force constants, as compared to those for distances and angles, is apparent.

While including the same CG torsional parameters, we actually considered three options for deriving the parameters for distances and angles: (a) 1G-fits both for distances and angles, (b) 3G-averages for bonds and 1G-fits for angles, and (c) 3G-averages both for distances and angles. In the following, the names of the various FF models discussed indicate the particular choice by “1–1,” “3–1,” or “3–3,” respectively. A “1–3” model based on 1G-fits for interdistances and 3G-averages for angles is of little interest, as explained in the next section, and, due to the substantial differences between the CG and AA distributions, it was abandoned altogether.

Standard Martini types and LJ parameters from atomistic structural data

Determining the nonbonded LJ parameters for a CG Martini model is nontrivial, since, by definition, the beads need to be included in standard types in order to benefit from compatibility with the Martini FF as a whole.

Searching for the optimal-type combinations, we identified our three bead types (PEI, PEP, and PEC) with a wide range of standard Martini types including small (S) and tiny (T) variants. As a simplification without notable impact (as shown by a wide body of test simulations), we assigned the same standard type (and implicitly the same LJ parameters) to the unprotonated bead PEI and the terminal PEC bead, however, with PEI and PEC carrying their real molecular masses and being subject to different bonded parameters. Indeed, merely acting as ending groups, the PEC beads only have a marginal influence on the chain behavior. More precisely, we tested for the neutral PEI bead several nonpolar types (Nda, Nd, N0, along with their S and T variants) and even a polar-type P2 (as suggested by

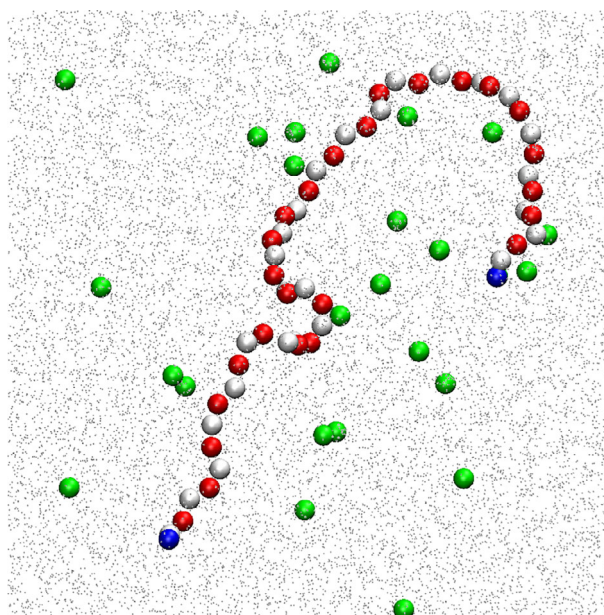


Figure 5. Snapshot from typical CG trajectory for the 1/2-uniformly protonated PEI 51-mer using polarizable water and the SNda-SQd-3-1-P FF model. The PEI beads are depicted in white, the PEP beads in red, the PEC beads in blue, and the neutralizing Cl^- ions in green. [Color figure can be viewed at wileyonlinelibrary.com]

Mahajan and Tang^[9]). For the protonated PEP bead (carrying unitary charge), we considered charged types (Qda, Qd, Q0, together with S and T variants), which reflect the hydrogen-bonding (donor) character of this group. Among all the considered Martini-type combinations for the PEI-PEP pair, we specifically included also those suggested by Wei and Luijten,^[7] that is, SNda-SQd, and by Mahajan and Tang, namely P2-Qd. Worth noting, while the first pair includes small types, the second, based on free energy considerations, operates with regular types.

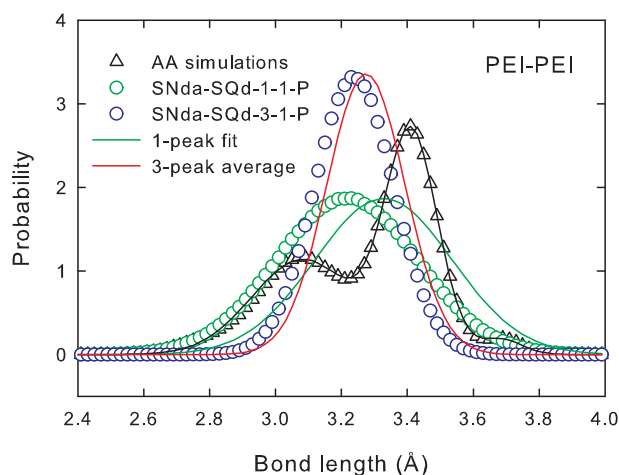


Figure 6. Probability distributions for the PEI-PEI distance. The AA results are depicted with triangles, the CG results obtained with polarizable water using the SNda-SQd-1-1-P and SNda-SQd-3-1-P FFs are represented with green and blue circles, respectively. The 1-Gaussian model is shown with green line and the 3-Gaussian-average model, with red line. [Color figure can be viewed at wileyonlinelibrary.com]

Given its crucial role in conferring realism to simulations of solvated systems with significant charge separations (as is, indeed, the case of protonated PEI chains), we mainly employed polarizable water. Yet, in an attempt to also provide a CG FF model for PEI for less expensive calculations, we also considered nonpolarizable (single-bead) water.

With a view to classify the different Martini-type combinations assigned to the PEI-PEP bead pair, we conducted for each of them massive CG MD simulations in conjunction with each of the three bonded parameter models ("1-1," "3-1," and "3-3," see previous section), both with polarizable and standard water. Specifically, the quality of the resulted FF models was assessed based on the average RMSD of the CG and AA gyration radii (R_g) and end-to-end distances (D_{ee}) for the entire RSS (12 combinations of PEI chain lengths and protonation patterns). The acronyms used further on for the various versions of FFs indicate the Martini types for the PEI-PEP pair, along with the bonded interaction model. For example, the FF model "SNda-SQd-3-1-P" assigns the small Martini types SNda and SQd to PEI (and also PEC) and PEP, respectively, using the bonded parameters obtained by using 3G-averages for bead inter-distances, 1G-fits for angles, and, in all cases, four-function fits for torsions. The trailing "P" indicates usage in tandem with polarizable CG water.

Figure 5 shows a typical snapshot from the 500-ns long CG trajectory run for the alternatively protonated PEI51 chain employing the SNda-SQd-3-1-P FF in conjunction with polarizable water and 25 neutralizing Cl^- ions.

A qualitative understanding of the manner in which the bonded parameter models work in conjunction with the standard Martini-type pairs assigned to PEI and PEP can be grasped from Figure 6, which shows probability distributions for the PEI-PEI distance. The AA reference results are depicted with triangles, while the profiles resulted from CG simulations using the SNda-SQd-1-1-P FF (SNda type for PEI, SQd type for PEP,

1G-fit functions both for distances and angles, and polarizable water) and the SNda-SQd-3-1-P FF are represented with green and blue circles, respectively. One can immediately notice that, as a result of the additional van der Waals contributions, the simulated CG probability distribution for the SNda-SQd-1-1-P FF (green circles) shifts quite substantially from the 1G bonded model (green line). Quite in contrast, the better localized CG probability distribution for the SNda-SQd-3-1-P FF (blue circles) is significantly more consistent both with the 3G-average model (red line) and the overall AA profile. This finding led us to no longer considering 1G-fits for distances, but only 3G-averages, that is, to drop the "1-1" model and exclusively rely on the "3-1" and "3-3" bonded models.

The effect of 3G-averaging versus 1G-fits on the simulated CG angular probability distributions is comparatively illustrated for the PEP-PEI-PEP angle in Figure 7, where the 1G-fit (green line) appears to follow more closely the AA distribution than the 3G-average (red line). Also, the CG distributions simulated with the FFs SNda-SQd-3-1-P (blue circles) and SNda-SQd-3-3-P (red circles), implementing the 1G and, respectively, the 3G approach for angles, obey the same ordering. These findings suggest the "3-1" model (3G-averages for distances and 1G-fits for angles) as the most appropriate for extracting bonded CG parameters. Nonetheless, as shown below, the "3-3" model remains a strong competitor, actually yielding the lowest RMSD between the AA and CG values of the gyration radius and end-to-end distance.

The simulated CG probability distribution for the PEI-PEI-PEI-PEI dihedral angle can be seen in Figure 8 to fairly reproduce the AA profile. This agreement is exhibited in qualitative terms by all tested FF models, since they are based on the same four-function fit for dihedrals. Quite in contrast, the torsional coordinates turn out to be very sensitive to the presence of protonated beads, and as shown by Figures S8 and S9, the CG distribution, albeit maintaining the overall aspect, departs both from the AA values and the fit model due to the additional charge involved.

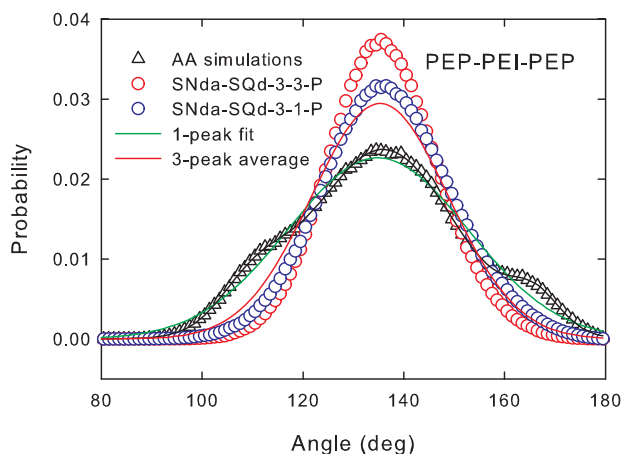


Figure 7. Probability distributions for the PEP-PEI-PEP angle. The AA results are represented with triangles, the CG results obtained with polarizable water using the SNda-SQd-3-3-P and SNda-SQd-3-1-P FFs are depicted with red and blue circles, respectively. The 1-Gaussian model is plotted with continuous green line and the 3-Gaussian-average model, with red line. [Color figure can be viewed at wileyonlinelibrary.com]

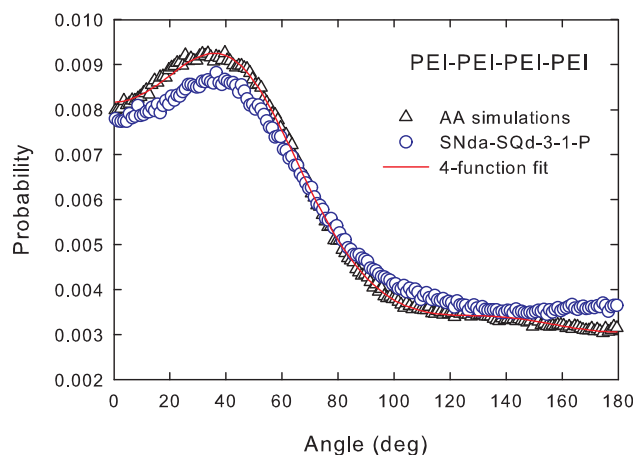


Figure 8. Probability distributions for the PEI-PEI-PEI-PEI dihedral angle from CG simulations with the SNda-SQd-3-1-P FF model and from AA simulations. The four-function fit model is plotted with red continuous line. [Color figure can be viewed at wileyonlinelibrary.com]

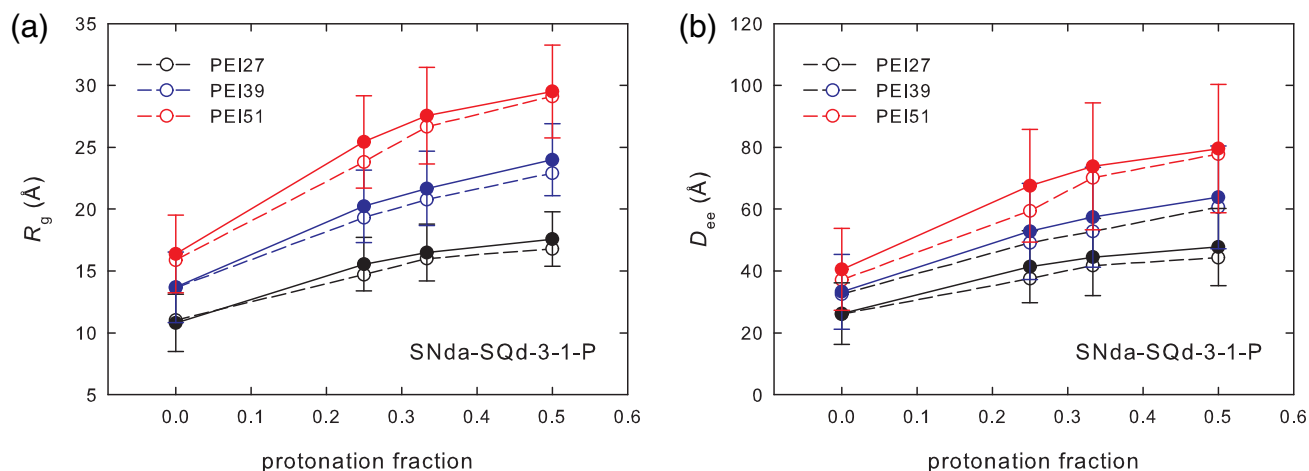


Figure 9. Radius of gyration a) and end-to-end distance b) for the PEI chains of the RSS using polarizable water and the SNda-SQd-3-1-P FF model. AA (CG) values are represented with empty (filled) circles and are connected with dotted (continuous) lines. [Color figure can be viewed at wileyonlinelibrary.com]

The CG probability distributions for the bead interdistances, angles, and dihedral angles not discussed above are presented in Supporting Information Figures S1–S7.

A reliable quantitative classification of the quality of the various CG FF models in reproducing AA features can be achieved based on *global* structural features of the PEI chains such as the gyration radius and the end-to-end distance, focusing on their dependence on the chain length and protonation pattern. This contrasts with other works, where rather the *local* environments are compared by the use of CG and AA radial distribution functions.

Figure 9a depicts the trajectory-averaged gyration radius for each of the 12 PEI polymers of the RSS, illustrating the smooth natural increase of the average spatial extent both with chain length and protonation fraction. The reference AA values are marked with empty circles and connected with dotted lines for each PEI chain size. The CG values (depicted with filled circles and connected with continuous lines) were extracted from 500-ns long trajectories using the SNda-SQd-3-1-P FF model with polarizable water, and can be seen to fairly follow the AA profiles, yet with a slight overestimation tendency of less than 5% (which indicates a slightly increased rigidity). A very similar behavior exhibits the end-to-end distance (see Fig. 9b), with CG-AA deviations rising to about 7%.

Table 2. RMSD of the CG and AA gyration radii (R_g) and end-to-end distances (D_{ee}), averaged over the entire RSS of 12 types of solvated PEI chains, for selected combinations of standard Martini types assigned to the PEI-PEP pair, with polarizable water, and using the “3–3” model for bonded interactions.

PEI/PEP	RMSD (R_g)			RMSD (D_{ee})		
	Qd	SQd	SQ0	Qd	SQd	SQ0
SNda	0.75	0.94	1.10	2.29	4.20	4.68
SN0	1.36	1.48	1.46	5.96	5.93	5.49
SNd	1.64	1.81	1.92	5.80	6.59	7.25
P2	3.19			10.08		

As stated above, we actually scanned a large set of Martini types for the PEI-PEP pair in combinations with the “3–1” and “3–3” models for bonded interactions and polarizable or non-polarizable water. The RMSD between the CG and AA gyration radii (R_g) and end-to-end distances (D_{ee}) for the most suitable Martini-type pairs are listed in Tables 2 and 4 for CG simulations with polarizable and nonpolarizable water, respectively. These results illustrate the use of the “3–3” model for bonded interactions, which yields the absolute lowest RMSD values. The contrasting presence of the P2-Qd pair (suggested by Mahajan and Tang^[9]) is only intended to illustrate a case of poor CG-AA agreement.

Optimal Martini FF models for PEI with polarizable

water. With polarizable water (Table 2), the lowest RMSD values, both for R_g and D_{ee} , can be seen to result for the SNda-Qd and SNda-SQd pairs (the second being also suggested by Wei and Luijten^[7]). These results are a clear indication that the

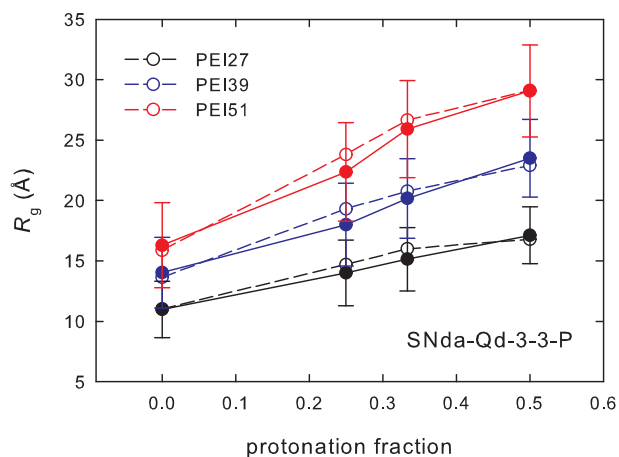
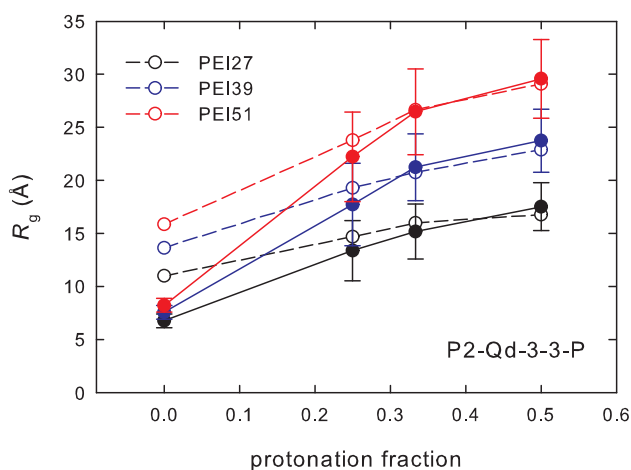


Figure 10. Radius of gyration for the RSS using polarizable water and the SNda-Qd-3-3-P FF model. AA (CG) values are represented with empty (filled) circles and are connected with dotted (continuous) lines. [Color figure can be viewed at wileyonlinelibrary.com]

Table 3. RMSD of the CG and AA gyration radii (R_g) and end-to-end distances (D_{ee}), averaged over the entire RSS of 12 types of solvated PEI chains, for the SNda-Qd and SNda-SQd standard Martini-type combinations assigned to the PEI-PEP pair, with polarizable water, and using the “3–1” and “3–3” models for bonded interactions.

Bonded model	RMSD (R_g)		RMSD (D_{ee})	
	SNda-Qd	SNda-SQd	SNda-Qd	SNda-SQd
“3–1”	0.92	0.83	2.78	3.81
“3–3”	0.75	0.94	2.29	4.20

**Figure 11.** Radius of gyration for the RSS using polarizable water and the P2-Qd-3-3-P FF model. AA (CG) values are represented with empty (filled) circles and are connected with dotted (continuous) lines. [Color figure can be viewed at wileyonlinelibrary.com]

PEI bead needs to be a “small” neutral type, which makes sense given the three-to-one bead mapping applied in this case. The somewhat better performance of the SNda-Qd pair (with only PEI as “small” type) can be judged from Figure 10, where the CG values of R_g appear to follow more closely the AA results. Nonetheless, the more uniform overall consistency of the CG and AA profiles for the SNda-SQd pair (with both PEI and PEP as “small” types) is apparent from Figure 9a.

In more quantitative terms, Table 3 lists the RMSD values for the SNda-Qd and SNda-SQd-type pairs in combinations with both the “3–1” and “3–3” bonded models. As an important finding, the best performance in reproducing the AA results with polarizable water (lowest RMSD both for R_g and D_{ee}) is achieved by the SNda-Qd-3-3-P and SNda-SQd-3-1-P FF models and Figures 9a and 10 illustrate precisely these cases.

The Martini-type combination P2-Qd suggested by Mahajan and Tang^[9] can be seen in Figure 11 to perform poorly for

nonprotonated or weakly protonated PEI chains in polarizable water. This behavior can be unequivocally ascribed to the choice of the regular polar-type P2, instead of a “small” neutral type, for the nonprotonated PEI bead. Indeed, the high P2–P2 interaction (Martini level II),^[15] favors artificial clustering of the PEI units and leads to excessively small gyration radii. More generally, assigning regular Martini types (such as Nda and P2) to the PEI bead causes non- or weakly protonated chains to collapse, so the use of a small S-type for PEI appears obligatory. It is also worth mentioning, that any attempt to involve “tiny” Martini types leads to significant RMSD values, making these types inadequate.

Optimal Martini FF model for PEI with nonpolarizable water.

Pursuing the idea of providing a CG FF for PEI to be used with standard water in expeditious, less expensive simulations, Table 4 indicates SN0–SQ0 as the optimal Martini-type combination for the PEI-PEP pair in combination with the “3–3” bonded model (resulting in the lowest RMSD both for R_g and D_{ee}). It should be noted that the RMSD values are substantially higher than those for polarizable water (Table 2). While the lowest RMSD (R_g) for polarizable water is 0.75 (for SNda-Qd), with standard water the minimum amounts to 2.38. The origin of this threefold increase of the RMSD emerges by inspecting Figure 12, where the degradation of the agreement between the CG and AA R_g values with increasing protonation fraction is obvious.

The reduction of the CG gyration radii as compared to the AA values for densely protonated PEI chains is a direct consequence of the increased electrostatic screening ($\epsilon_r = 15$) which is customary applied to avoid spurious charge clustering. This has, evidently, no effect on nonprotonated chains, for which there is an excellent agreement between the CG and AA results. It should also be emphasized (from Supporting Information Table S2) the significantly lower Martini interaction level for the SN0–SQ0 pair in standard water ($\sigma = 0.43$ nm, $\epsilon = 2.6$ kJ mol⁻¹)

Table 4. RMSD of the CG and AA gyration radii (R_g) and end-to-end distances (D_{ee}), averaged over the entire RSS of 12 types of solvated PEI chains, for selected combinations of standard Martini types assigned to the PEI-PEP pair, with nonpolarizable water, and using the “3–3” model for bonded interactions.

PEI/PEP	RMSD (R_g)				RMSD (D_{ee})			
	SQ0	SQd	Q0	Qd	SQ0	SQd	Q0	Qd
SN0	2.38	3.44	3.64		7.68	11.19	11.91	
SNd	3.64	4.84	4.86		12.18	16.05	15.96	
SNda	3.95	5.17	5.45	9.16	13.13	16.71	18.27	30.27

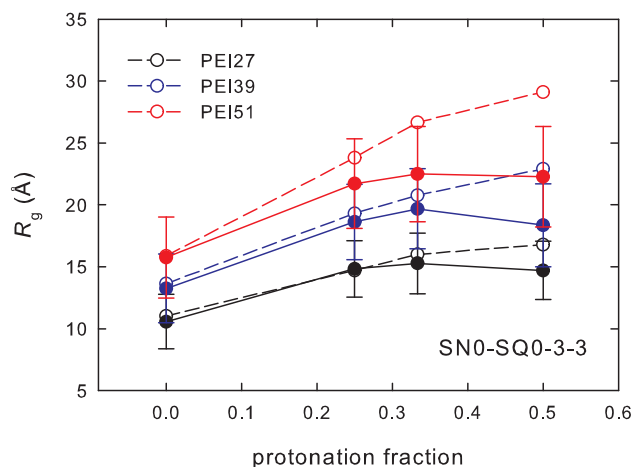


Figure 12. Radius of gyration for the RSS using *nonpolarizable* water and the SN0-SQ0-3-3 FF model. AA (CG) values are represented with empty (filled) circles and are connected with dotted (continuous) lines. [Color figure can be viewed at wileyonlinelibrary.com]

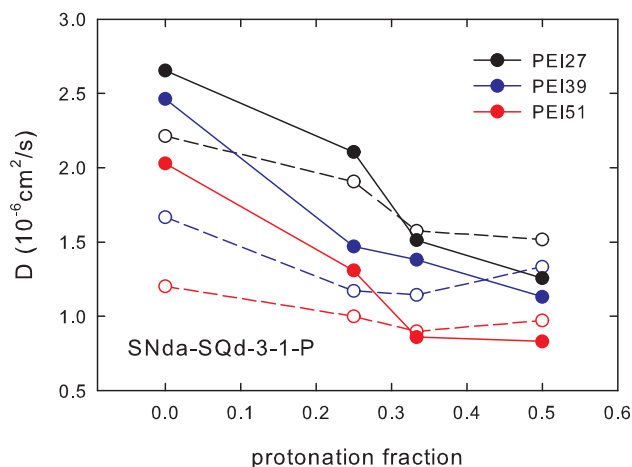


Figure 13. Diffusion coefficients for the RSS with the SNda-SQd-3-1-P FF model. AA (CG) values are represented with empty (filled) circles and are connected with dotted (continuous) lines. [Color figure can be viewed at wileyonlinelibrary.com]

as compared to the SNda-Qd and SNdq-SQd pairs with polarizable water ($\sigma = 0.47$ nm, $\epsilon = 5.6$ kJ mol⁻¹).

The Martini-type pair SNda-SQd, which was found to perform very well with polarizable water, is seen to perform poorly with standard water, with a more than fourfold increase of the RMSD as compared to SN0-SQ0. Hence, the optimal FF model for PEI in standard (nonpolarizable) water is SN0-SQ0-3-3, yet it can be reliably employed only for weakly protonated PEI chains, i.e. for protonation fractions lower than 1/4.

Concluding the discussion on the parametrization of the Martini FF for PEI, we summarize the optimal models in Table 5. The Martini interaction levels for the PEI-PEP pairs are to be taken from Marrink et al.^[15] (with standard water) and Yesylevskyy et al.^[19] (with polarizable water), while the bonded parameters are those listed in Table 1 for bead distances and angles, and in Supporting Information Table S1 for dihedral angles.

As a supplementary indication for the realism of the developed CG models, we present in Figure 13 center-of-mass diffusion coefficients for each of the PEI chains of the RSS, extracted from simulations based on the SNda-SQd-3-1-P FF model. We actually computed the diffusion coefficients,

known to be numerically very sensitive, using the straightforward implementation of Einstein's formula without any sophisticated sampling technique. As can be seen, our CG results reproduce semi-quantitatively the AA values (which are themselves affected by some fluctuations), with an overestimation tendency for lower protonations, but preserving the proper ordering and the correct, decreasing protonation and chain length dependencies. Specifically, while the experimental diffusion coefficient (1.2×10^{-6} cm² s⁻¹) reported by Clamme et al.^[25] for branched PEI (molecular weight 2500) is nicely reproduced by our AA value for the unprotonated PEI51 (molecular weight 2226), it is overestimated by a factor of about 2 by our CG result. In fact, it is a matter of common knowledge that the larger CG bead sizes result in smoother energy landscapes and artificially increased dynamics. This calls for the time scale to be reinterpreted, or, equivalently, for the diffusion coefficients to be scaled down, as recommended by Marrink et al.^[14]

Formation of DNA-PEI complexes

An illustrative way to put the developed Martini FF models to test is by simulating the formation of solvated DNA-PEI complexes. Mainly using the new SNda-SQd-3-1-P FF model and the standard Martini FF for DNA,^[17] we performed CG MD simulations of a double Drew-Dickerson DNA-dodecamer (with one of the strands CGCGAATTCGCG-CGCGAATTCGCG), enclosed in a cubic box of size 6.76 nm, constrained along the z-axis, and subject to periodic boundary conditions to mimic an infinitely long chain. We distributed various numbers of initially linear PEI 15-mers circularly, parallel to the DNA-axis at a distance of 25 Å. We CG the atomistic DNA-PEI system and solvated it, adding a suitable number of neutralizing Na⁺ or Cl⁻ ions. For each particular number of PEI chains and protonation fractions 1/2 or 1/4, we conducted Gromacs simulations spanning 500 ns, using the main parameters specified under "Methodology" section.

Table 5. Optimal Martini FF models for solvated PEI chains, in increasing order of the RMSD between the CG and AA values of the gyration radii and end-to-end distances for the RSS.

Model acronym	Martini type		Boltzmann inversion			Water model
	PEI	PEP	Distances	Angles	Dihedrals	
SNda-Qd-3-3-P	SNda	Qd	3G	3G	4F	Polarizable
SNda-SQd-3-1-P	SNda	SQd	3G	1G	4F	Polarizable
SN0-SQ0-3-3	SN0	SQ0	3G	3G	4F	Nonpolarizable

1G, 1-Gaussian-fit; 3G, 3-Gaussian-average; 4F, 4-function fit.

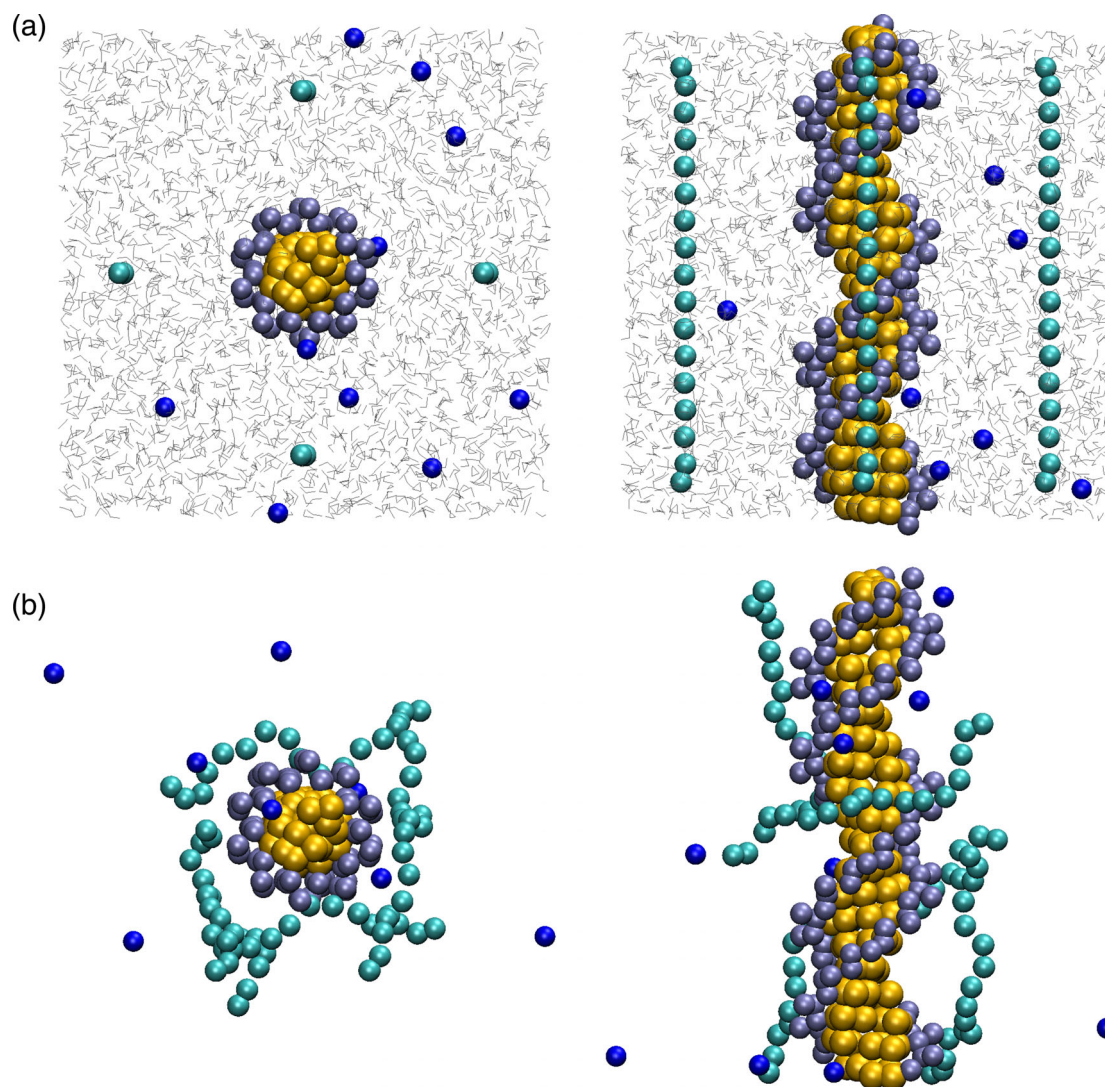


Figure 14. Top view and side view of a double Drew–Dickerson DNA–dodecamer with four alternatively protonated PEI15 chains, 10 neutralizing Na^+ ions, and 2565×3 polarizable water beads, enclosed in a cubic box of size 6.9 nm: a) initial configuration and b) snapshot from a CG simulation (water is not shown), using the new SNda–SQd–3–1–P Martini FF model. [Color figure can be viewed at [wileyonlinelibrary.com](#)]

Figures 14a and 14b show for a system with four 1/2-protonated PEI15 chains, 2565 polarizable water bead triplets, and 10 neutralizing Na^+ ions (a) the initial configuration and (b) a snapshot from a CG simulation, illustrating the uniform condensation of the PEI chains about the DNA helix.

To characterize the formation of DNA–PEI complexes, we analyzed the affinity between the phosphate groups (BB1 beads, as defined by Uusitalo et al.^[17]) of DNA and the protonated PEP beads of the PEI chains, using the potential of mean force (PMF),

$$\text{PMF} = -k_B T \log P_{\text{BB1-PEP}}, \quad (12)$$

defined in terms of the normalized probability distribution of the radial BB1–PEP distance $P_{\text{BB1-PEP}}$ (k_B is Boltzmann's constant and T is the temperature). Figure 15 depicts the PMF for systems composed of 2, 4, 6, and 8 alternatively protonated, and, respectively, 1/4-protonated PEI 15-mers. It can be noticed that all the PMF profiles show the closest minimum at about 0.46 nm.

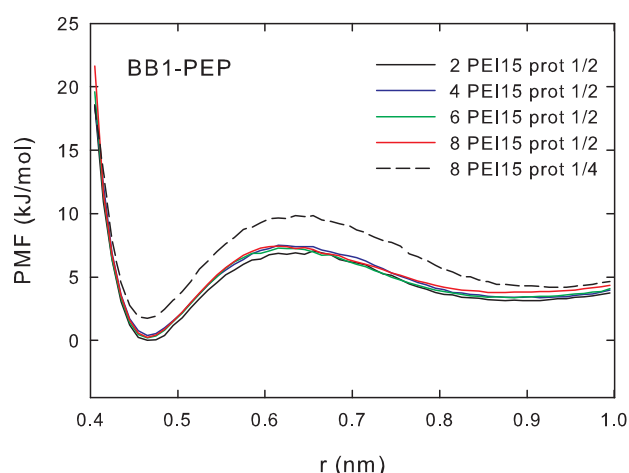


Figure 15. PMF profiles from GG simulations for the interaction between the phosphate groups (BB1 beads) of a double Drew–Dickerson DNA–dodecamer and the protonated PEP beads of 2, 4, 6, and 8 alternatively protonated, and, respectively, 1/4-protonated PEI 15-mers. [Color figure can be viewed at [wileyonlinelibrary.com](#)]

While the profiles for the 1/2-protonated PEI chains are practically indiscernible, essentially exhibiting the same affinity pattern of the PEP beads for the BB1 beads, the dotted curve corresponding to the 1/4-protonated chains is shifted to higher values. The higher affinity in the case of the 1/2-protonation can be readily explained based on the fact that the nominal distance between consecutive PEP beads is comparable to that between BB1 phosphates beads along the DNA backbone, offering an energetically more favorable PEP–BB1 pairing pattern. Lower protonation fractions result in a less efficient packing of the DNA helix by the PEI chains.

Referring to the N/P ratio of positively charged PEI amino groups (N) to negatively charged DNA phosphate groups (P), the enhanced complexation of DNA for alternative protonation ($N/P = 1.47$, for the eight PEI15 chains considered for illustration) as compared to 1/4-protonation ($N/P = 0.63$) obviously correlates with N/P ratios higher than 1. This result is consistent with relative fluorescence measurements (see Fig. 2 of Kunath et al.^[26]), in which the DNA complexation efficiency in the presence of low-molecular-weight PEI is demonstrated to increase with the N/P ratio, showing saturation for ratios exceeding 2.

A more detailed analysis regarding the formation of DNA–PEI complexes, including DNA–PEI condensation results for significantly larger systems, will be offered in a follow-up paper.

Conclusions

We report a new CG Martini FF model for PEI chains, with variants to be respectively used in conjunction with polarizable and standard water. The bonded interactions for bead interdistances, angles, and dihedral angles were parameterized by Boltzmann inversion from bead-based probability distributions yielded by accurate AA simulations performed using our recently published CHARMM FF for PEI. Assignment of standard Martini types to the PEI beads (and implicitly of LJ parameters) was achieved by matching AA gyration radii, end-to-end distances, and probability distributions for a representative set of 12 solvated PEI chains (of three lengths and four protonation fractions) to the CG results obtained from comprehensive MD simulations scanning large sets of Martini-type combinations. One of our optimal Martini FF models relies on a pair of standard Martini bead types that was also proposed by Wei and Luijten,^[7] involving, however, a significantly more realistic bonded parameter set.

Essential modeling aspects affecting the realism of the developed FF models, such as the relevance of polarizable water or options for electrostatics, are discussed in detail.

Combining our Martini FF for PEI with the standard Martini FF for DNA of Uusitalo et al.,^[17] we carried out MD simulations of solvated DNA–PEI systems. Focusing on the distribution of distances between the protonated units of PEI (PEP) and the negative phosphate groups of DNA (BB1), we discuss the formation of DNA–PEI complexes in terms of the PMF for the PEP–BB1 interaction in dependence of PEI chain size and protonation pattern. Besides providing insights into the

formation of the DNA–PEI polyplexes, our developed FF models open the way for ample, realistic MD simulations of DNA–PEI condensation.

Acknowledgments


This work was supported by a grant of the Romanian National Authority for Scientific Research and Innovation, CNCS—UEFISCDI (PN-III-P4-ID-PCE-2016-0474).

Author Contributions

AEA and RIC contributed to defining the Martini mapping schemes, performing MD simulations for PEI, interpreting the results, and writing the article. TAB conceived the Martini PEI model, wrote the scripts for coarse-graining the systems, input preparation, and trajectory analysis, performed and post-processed the bulk of the MD simulations, prepared the graphical output, and largely wrote the article.

Keywords: cationic polymers · polyethyleneimine · coarse-grained force fields · molecular dynamics

How to cite this article: T. A. Beu, A.-E. Ailenei, R. Costinaş. *J. Comput. Chem.* **2019**, 9999, 1–13. DOI: 10.1002/jcc.26110

 Additional Supporting Information may be found in the online version of this article.

- [1] T. A. Beu, A. Farcaş, *J. Comput. Chem.* **2017**, *38*, 2335.
- [2] T. A. Beu, A.-E. Ailenei, A. Farcaş, *J. Comput. Chem.* **2018**, *39*, 2564.
- [3] T. A. Beu, A.-E. Ailenei, A. Farcaş, *Chem. Phys. Lett.* **2019**, *714*, 94.
- [4] A. F. Jorge, R. S. Dias, A. A. C. C. Pais, *Biomacromolecules* **2012**, *13*, 3151.
- [5] J. Cai, G. Chen, R. Jin, C. Deng, S. Huang, X. Yuan, G. Chen, J. Zhao, Z. Wang, H. Ai, *J. Ind. Eng. Chem.* **2019**, *76*, 188.
- [6] J. D. Ziebarth, Y. Wang, *J. Phys. Chem. B* **2010**, *114*, 6225.
- [7] Z. Wei, E. Luijten, *J. Chem. Phys.* **2015**, *143*, 243146.
- [8] J.-M. Y. Carrillo, M. E. Potter, M. A. Sakwa-Novak, S. H. Pang, C. W. Jones, B. G. Sumpter, *Langmuir* **2017**, *33*, 5412.
- [9] S. Mahajan, T. Tang, *J. Comput. Chem.* **2019**, *40*, 607.
- [10] C. Sun, T. Tang, H. Uludağ, J. E. Cuervo, *Biophys. J.* **2011**, *100*, 2754.
- [11] A. D. MacKerell, N. Banavali, N. Foloppe, *Biopolymers* **2001**, *56*, 257.
- [12] A. D. MacKerell, D. Bashford, M. Bellott, R. L. Dunbrack, J. D. Evanseck, M. J. Field, S. Fischer, J. Gao, H. Guo, S. Ha, D. Joseph-McCarthy, L. Kuchnir, K. Kuczera, F. T. K. Lau, C. Mattos, S. Michnick, T. Ngo, D. T. Nguyen, B. Prodhom, W. E. Reiher, B. Roux, M. Schlenkrich, J. C. Smith, R. Stote, J. Straub, M. Watanabe, J. Wiórkiewicz-Kuczera, D. Yin, M. Karplus, *J. Phys. Chem. B* **1998**, *102*, 3586.
- [13] K. Vanommeslaeghe, E. Hatcher, C. Acharya, S. Kundu, S. Zhong, J. Shim, E. Darian, O. Guvench, P. Lopes, I. Vorobyov, A. D. MacKerell, Jr., *J. Comput. Chem.* **2010**, *31*, 671.
- [14] S. J. Marrink, A. H. de Vries, A. E. Mark, *J. Phys. Chem. B* **2004**, *108*, 750.
- [15] S. J. Marrink, H. J. Risselada, S. Yefimov, D. P. Tieleman, A. H. de Vries, *J. Phys. Chem. B* **2007**, *111*, 7812.
- [16] L. Monticelli, S. K. Kandasamy, X. Periole, R. G. Larson, D. P. Tieleman, S.-J. Marrink, *J. Chem. Theory Comput.* **2008**, *4*, 819.
- [17] J. J. Uusitalo, H. I. Ingólfsson, P. Akhshi, D. P. Tieleman, S. J. Marrink, *J. Chem. Theory Comput.* **2015**, *11*, 3932.
- [18] D. Reith, M. Pütz, F. Müller-Plathe, *J. Comput. Chem.* **2003**, *24*, 1624.
- [19] S. O. Yesylevskyy, L. V. Schäfer, D. Sengupta, S. J. Marrink, *PLoS Comput. Biol.* **2010**, *6*, 1.
- [20] J. Michalowsky, L. V. Schäfer, C. Holm, J. Smiatek, *J. Chem. Phys.* **2017**, *146*, 054501.

- [21] J. C. Phillips, R. Braun, W. Wang, J. Gumbart, E. Tajkhorshid, E. Villa, C. Chipot, R. D. Skeel, L. Kale, K. Schulten, *J. Comput. Chem.* **2005**, *26*, 1781.
- [22] B. Hess, C. Kutzner, D. van der Spoel, E. Lindahl, *J. Chem. Theory Comput.* **2008**, *4*, 435.
- [23] S. Pronk, S. Páll, R. Schulz, P. Larsson, P. Bjelkmar, R. Apostolov, M. R. Shirts, J. C. Smith, P. M. Kasson, D. van der Spoel, B. Hess, E. Lindahl, *Bioinformatics* **2013**, *29*, 845.
- [24] M. J. Abraham, T. Murtola, R. Schulz, S. Páll, J. C. Smith, B. Hess, E. Lindahl, *SoftwareX* **2015**, *1–2*, 19.
- [25] J. P. Clamme, J. Azoulay, Y. Mely, *Biophys. J.* **2003**, *84*, 1960.
- [26] K. Kunath, A. Harpe, D. Fischer, H. Petersen, U. Bickel, K. Voigt, T. Kissel, *J. Control. Release* **2003**, *89*, 113.

Received: 23 September 2019

Revised: 30 October 2019

Accepted: 30 October 2019
